

# Large scale modeling of the transport, chemical transformation and mass budget of the sulfur emitted during the April 2007 eruption of Piton de la Fournaise.

P. Tulet<sup>1,2</sup> and N. Villeneuve<sup>3</sup>

<sup>1</sup>LACy (CNRS, Université de La Réunion, Météo-France), 15 avenue René Cassin, 97715 Saint-Denis Messag., France

<sup>2</sup>CNRM/GAME (CNRS, Météo-France), 42, Avenue Gaspard Coriolis, 31057 Toulouse, France

<sup>3</sup>US140 ESPACE (Centre IRD de La Réunion), BP172, 97492 Saint-Denis, France

**Abstract.** In April 2007, the Piton de la Fournaise volcano (Réunion island) entered into its biggest eruption recorded in the last century. Due to the absence of a sensors network in the vicinity of the volcano, the estimation of the degassing during the paroxysmal phase of the event has not been performed. Nevertheless, the SO<sub>2</sub> plume and aerosols have been observed by the OMI and CALIOP space sensors, respectively. The mesoscale chemical model MesoNH-C simulates the observed bulk mass of SO<sub>2</sub> and the general shape of the SO<sub>2</sub> plume spreading over the Indian Ocean. Moreover, an analysis of the SO<sub>2</sub> plume budget estimates a total SO<sub>2</sub> release of 230 kt, among of which 60 kt have been transformed into H<sub>2</sub>SO<sub>4</sub>. 27 kt of SO<sub>2</sub> and 21 kt of H<sub>2</sub>SO<sub>4</sub> have been deposited at the surface by dry deposition. With this top down approach, the temporal evolution of the SO<sub>2</sub> emission has been estimated during the most active period of the eruption. The peak of degassing was estimated at 1800 kg s<sup>-1</sup> in the morning of April 6. The temporal evolution of SO<sub>2</sub> emission presented here can also be used for local studies.

as has happened recently during Eyjafjöll's 2010 eruption in Iceland (Seifert et al., 2010). For these reasons, the understanding and forecasting of the volcanic plumes are still major challenges for atmospheric sciences and risk mitigation.

In the atmosphere science of volcanic plumes, sulfur dioxide (SO<sub>2</sub>) is the most commonly measured gas (Thomas et al., 2009). Resulting from the oxidation of sulfur present in the magma, the degassing of SO<sub>2</sub> is a robust indicator of eruptive activity and sheds light on magma storage (Edmonds et al., 2003; Sutton et al., 2001). In the atmosphere, oxidation of SO<sub>2</sub> into sulfate forms aerosols by homogeneous nucleation (Kulmala et al., 1998) or deposition on pre-existing aerosols (Seinfeld and Pandis, 2006; Martin et al., 2008; Stevenson et al., 2003). Through aqueous processes, SO<sub>2</sub> can also form acid rain (Hoffman et al., 1985; Stevenson et al., 2003). On the global scale, Penner et al. (2001) have estimated that the source of volcanic sulfur in the atmosphere ranges from 6 to 20 Tg of sulfur per year (Tg(S) yr<sup>-1</sup>). This amount of release is non-negligible compared to the anthropogenic fluxes estimated between 70 and 100 Tg(S) yr<sup>-1</sup>, which corresponds to 70 % of the total sulfur emissions.

## 1 Introduction

Volcanoes represent one of the most significant natural sources of pollutants in the atmosphere, both during and between eruptions (Mather et al., 2005). Large explosive eruptions such as El Chichón in 1982 (Pollack et al., 1983; Hoffman, 1987) or Mount Pinatubo in 1991 (McCormick et al., 1995; Robock, 2002) have highlighted their impacts on the earth's radiative balance through the injection of large quantities of aerosol into the troposphere and the lower stratosphere (Delmelle et al., 2002; Oppenheimer et al., 2003; Arellano et al., 2008). In addition, volcanic emissions can also cause serious perturbations in air traffic

For many years, satellite-based measurements of volcanic SO<sub>2</sub> emissions were limited to major eruptions linked to large production of SO<sub>2</sub> and big plumes (Carn et al., 2008). Until recently, most measurements of volcanic SO<sub>2</sub> fluxes between two eruption events, or measurements of effusive volcanoes, were based on ground or airborne instrumentation (Carn et al., 2007). Even though most space-based SO<sub>2</sub> measurements were useful for volcanic hazard mitigation (including aviation consequences) and for tracking volcanic clouds (Krueger et al., 1995; Afe et al., 2004; Khokhar et al., 2005), a significant advance was introduced with recently launched sensors (Carn et al., 2008).

---

Correspondence to: P. Tulet  
(pierre.tulet@univ-reunion.fr)

In this context, the amount of  $\text{SO}_2$  released into the atmosphere by the eruption of Piton de la Fournaise in April 2007 at La Réunion needs to be estimated for two reasons. First, Piton de la Fournaise is one of the world's most active volcanoes (Lenat and Bachelery, 1987) with an average of one eruption every eight months in the last fifty years (Peltier et al., 2009). Secondly, the April 2007 eruption is the largest eruption of Piton de la Fournaise in at least one century (Deroussi et al., 2009). At least  $180 \cdot 10^6 \text{ m}^3$  of lava was estimated to be produced during this eruption (of which half stayed on the Le Grand Brûlé area (Staudacher et al., 2009) and half went into the sea (SaintAnge, 2009)).

Most of the time, the eruptions of the Piton de la Fournaise do not produce significant quantities of ash and sulfur. In the literature, only few examples reference such activity, most often associated with historic caldera collapses. This kind of activity has been observed from the presence of volcanic ash rather than sulfur. Khokhar et al. (2005), Bhugwant et al. (2008) and Staudacher et al. (2009) are the only references to an observed plume rich in sulfur that was produced by an eruption of Piton de la Fournaise. Except in urban areas, no ground instruments continuously measured  $\text{SO}_2$  during the paroxysmal stage of the eruption. As a consequence, the sulfur degassing of Piton de la Fournaise has not been estimated. The main objective of this study is to estimate the  $\text{SO}_2$  release using both large scale satellite observations and a top-down modeling approach. This paper is an extension of preliminary  $\text{SO}_2$  mass estimates published on-line during and just after the April 2007 eruption, using the OMI, SCIAMACHY and GOME2 sensors (<http://so2.umbc.edu/omi/pix/special/2007/piton/piton04.php> and <http://sacs.aeronomie.be>).

This paper is organized as follows. Section 2 focuses on the eruption phenomenon. An analysis of the  $\text{SO}_2$  plumes observed by satellites is given in Section 3. Then, the numerical methods (Section 4) and the simulation results (Section 5) are presented. The last section is devoted to quantifying the mass budget of the volcanic sulfur and to estimate the  $\text{SO}_2$  emitted during the main eruptive period.

## 2 Description of the Piton de la Fournaise volcano eruption (April 2007)

The April 2, 2007 eruption is the largest eruption of Piton de la Fournaise volcano on Réunion island in at least one century (Deroussi et al., 2009). The associated collapse of the summit caldera caused significant morphological change (Michon et al., 2007). Due to this abnormal phenomenon and its large impact on the environment and on civil protection policy, this eruption is very well described in literature. The most important phases are summarized below. The April 2, 2007 eruption was preceded by two short erup-

tive events (lasting only a few hours) on February 18 and on March 30. At 06 UTC on April 2, a new eruption started along a 1 km long fissure, located on the lower south-eastern part of the Enclos (called Le Grand Brûlé) at only 590 m above sea level (asl), 7 km away from the summit and 3 km from the coast. The beginning of the April 2, 2007 eruption was characterized by 50 m high continuous lava fountains feeding voluminous lava flows (Michon et al., 2007). The Observatoire Volcanologique du Piton de la Fournaise recorded high seismicity related to the opening of the eruptive fissure (Staudacher et al., 2009). For a few hours on April 3 activity dramatically decreased before gradually re-summing until it reached a maximum at mid-day on April 6. This period was observed by remote sensing instruments. In fact, Coppola et al. (2009) estimated a significant increase of the lava flow rate between the April 3 and the April 5, from  $55$  to  $75 \text{ m}^3 \text{ s}^{-1}$ , by radiance analyses of the MODIS sensors. The first consequence of the vent location near the coast is the rapid and early entrance of the lava flow into seawater. This produced a large acid water vapour plume ( $\text{pH} < 2$ ), rich in chlorine and sulfur (Staudacher et al., 2009). On April 5 at 20:48 UTC, an earthquake of magnitude 3.2 coincided with the onset of a caldera collapse (Michon et al., 2007). A geodetic network recorded an inward deformation prior to the earthquake, followed by a sudden outward displacement of 10-20 cm (Peltier et al., 2009). From 20:48 UTC on April 5 until 00 UTC on April 7, the nature of the activity changed (Michon et al., 2007). Analysis of geophysical network signals allowed the determination of cycles characterized by variations in seismic activity and by deformation (progressive inward displacement ending in a strong outward motion) (Michon et al., 2007, 2009; Staudacher et al., 2009; Peltier et al., 2009). These authors interpreted such cycles as a result of pressure variations in the magma chamber causing a subsequential formation of the caldera. Output flow rates (greater than  $200 \text{ m}^3 \text{ s}^{-1}$ ) have been estimated by field observations, with a maximum during April 6 (Coppola et al., 2009). We consider this value to be underestimated. Nevertheless, observations clearly showed that the maximum activity at the eruption location (higher degassing, higher lava fountains and higher output flow rate) coincided with a higher seismic activity signature.

Figure 1 illustrates the volcanic event during the maximum stage. Figure 1a and 1b show the evolution between the afternoon of April 5 (Fig. 1a) when the activity increased and the afternoon of April 6 (Fig. 1b) at the collapse of the caldera. For the Figure 1c, the camera was installed near the Piton des Neiges summit, 27 km from Piton de la Fournaise summit and 37 km from the coast at Le Grand Brûlé. The ash plume (gray) close to Piton de la Fournaise summit is associated to one of the caldera collapses. Note that this ash plume has a relatively small extent. Furthermore the location of this ash plume is well separated from the  $\text{SO}_2$  one. This is due to the fact that the  $\text{SO}_2$  emission is linked to the degassing of the lava flow which started several kilometers from the crater. As

observed in Figure 1c, the SO<sub>2</sub> plume (orange) spreads out at a constant altitude. The water vapour plume (white) is a result of the lava flow entering into the sea. Note on Figure 1d that the volcanic activity dramatically decreases and the lava flow reaches its maximum lateral and longitudinal extents. This stage of the eruption became more "typical" compared to usual eruptions of Piton de la Fournaise. On April 10 between 08 and 11 UTC a rapid decrease in seismicity was followed by an 8-hour break. From 19:00 UTC activity resumed. On April 12 between 11 and 14 UTC a new collapse coevals with a high output flow rate and a small ash plume dispersion. Subsequently, activity remained stable until the end of the eruption. On April 28, several days after the paroxysmal stage, the Observatoire Réunionnais de l'Air (ORA) measured 2500  $\mu\text{g m}^{-3}$  of SO<sub>2</sub> in the village of Le Tremblet, which is located close to the volcano (Bhugwant et al., 2008).

### 3 Large scale transport of SO<sub>2</sub>

#### 3.1 Total column from OMI

OMI, onboard EOS/Aura, is an hyperspectral UV/Visible spectrometer with a 2600 km swath and a  $13 \times 24$  km<sup>2</sup> (at nadir) footprint size. Since July 2004, it allows a daily and contiguous global mapping of ozone and trace gases including SO<sub>2</sub>, NO<sub>2</sub>, and BrO (Carn et al., 2007). The retrieval method used in this study follows the algorithm described by Krotkov et al. (2006) and Yang et al. (2009) and has been validated by Krotkov et al. (2008). OMI SO<sub>2</sub> level 2 data products (OMSO<sub>2</sub> V003) used in our analyses are available on NASA's Goddard Earth Sciences Data and Information Services Center website ([http://disc.sci.gsfc.nasa.gov/Aura/data-holdings/OMI/omso2\\_v003.shtml](http://disc.sci.gsfc.nasa.gov/Aura/data-holdings/OMI/omso2_v003.shtml)). For each scene Goddard Earth Sciences Data provides four different estimates of the SO<sub>2</sub> column density using two different algorithms. Since OMSO<sub>2</sub> V003, the Planetary Boundary Layer (PBL) SO<sub>2</sub> columns that correspond to Center Mass Altitude (CMA) of 900 m asl are produced using the Band Residual Divergence (BRD) algorithm (Krotkov et al., 2006). The three other different estimates of the column density of SO<sub>2</sub> are produced with the Linear Fit algorithm (Yang et al., 2007): (i) lower tropospheric level plume (TRL) which corresponds to a CMA of 2500 m asl; (ii) middle tropospheric level SO<sub>2</sub> column (TRM), corresponding to CMA of 7500 m asl; and (iii) upper tropospheric and stratospheric (STL), corresponding to CMA of 17,000 m asl.

Figure 2 represents the evolution of the SO<sub>2</sub> plume, superimposed on Meteosat 7 satellite images (visible channel) for the period 4 to 9 April, 2007. The OMI data products are interpolated by Kriging method on a  $13 \times 24$  km<sup>2</sup> grid. The domain of interpolation covers a large part of the Indian Ocean ( $28.6^{\circ}\text{S} - 10.9^{\circ}\text{S}$ ;  $40.78^{\circ}\text{E} - 71.22^{\circ}\text{E}$ ). For April

4 and 5, SO<sub>2</sub> burden measurements are determined at the TRL (Fig. 2.a and b). For the rest of the eruptive period, a weighted value between TRM and TRL column is used (Fig. 2.c-f). These choices are justified by the location of SO<sub>2</sub> in the mid-troposphere after April 6 (CMA estimated at 6000 m, see next Section).

The presence of cloudy areas generates uncertainties for SO<sub>2</sub> quantification. In these regions, the SO<sub>2</sub> burden observed in Figure 2 only corresponds to the mass located over the top of the clouds which can cause an underestimation of the SO<sub>2</sub>. On the contrary, the cloud albedo can artificially increase the retrieved SO<sub>2</sub> values. In some cases pixel values can be negative. Georgoulis et al. (2009) assumed that negative SO<sub>2</sub> total column values are linked to a low amount of SO<sub>2</sub>. As a consequence, the negative values are removed in computations. On April 4, the SO<sub>2</sub> plume observed by OMI at 11 UTC is low, reaching 1 Dobson Unit (1 DU corresponding to  $2.68 \times 10^{16}$  molecules cm<sup>-2</sup>) and spreading about 2° west from La Réunion. The SO<sub>2</sub> increases on April 5 at 10 UTC, up to 70 DU (locally reaching 200 DU) to the west of La Réunion. The SO<sub>2</sub> is also advected at large distance to the west, close to the east coast of Madagascar, where the value of SO<sub>2</sub> is close to 2 DU.

April 6 (11 UTC) is the day when Piton de la Fournaise's main summit crater (Dolomieu) collapses, and significant quantities of lava are emitted (section 2). Unfortunately, for the quantification of SO<sub>2</sub>, two constraints have to be considered. First, the satellite track was far from the zenith of the main plume. As a consequence, the footprint size increases to  $13 \times 42$  km<sup>2</sup> and the accuracy of the data is lowered. Second, this day is also marked by the presence of clouds over La Réunion which prevents a complete detection of the SO<sub>2</sub> by OMI (Fig. 2.c). The maximum value of 12 DU observed in this area is probably largely underestimated and corresponds only to the SO<sub>2</sub> located above the clouds. Nevertheless one can note on Figure 2.c that the plume intensifies and spreads toward the west, close to the eastern coast of Madagascar, to the north and to the east of La Réunion, reaching Mauritius (15 DU). Considering that the lower tropospheric trade winds (Diab et al., 2004) are from the southeast, the presence of the plume in the eastern and northern areas around La Réunion indicates that the SO<sub>2</sub> plume has been transported above the inversion layer where wind directions are reversed. On April 7 at 10 UTC (Fig. 2.d), the plume observed by OMI has intensified. It was advected to the north of La Réunion and then moved eastward. The plume is detected at 83° E, 2800 km far away from Piton de la Fournaise. The integrated column of SO<sub>2</sub> is significant, with 50 DU over La Réunion, 40 DU in the northern branch and about 15-20 DU in the eastern branch at 65° E. A gap in the plume shape is noticeable over the area north of Mauritius, and is probably due to the presence of clouds. Close to Madagascar a second SO<sub>2</sub> (2 DU) plume corresponds to the western branch of the April 6 plume. The

size and concentration of the SO<sub>2</sub> plume detected far from La Réunion suggest that the SO<sub>2</sub> release on April 6 was considerable.

On April 8 and 9, the plume decreases to a maximum of 7 DU (Fig. 2.e) and 12 DU (Fig. 2.f), respectively. This second maximum of 12 DU located at 16° S and 58° E is puzzling given the fact that such strong values are not observed upstream in the plume on April 8. Thus, it implies that some plumes of SO<sub>2</sub> are masked by the presence of clouds. In this latter period, the plume extends over the Indian Ocean from 48° E on April 8, to 95° E on April 9 (not shown). Above Madagascar, the presence of a cloud system seems to interact with the western part of the plume.

### 3.2 Plumes altitudes from CALIPSO

On the CALIPSO satellite, the Cloud-Aerosol Lidar with Orthogonal Polarization (CALIOP) provides high-resolution vertical profiles (100 m footprint size) of aerosol and clouds. This sensor allows the discretization of cloud phase and the identification of the presence of non-spherical aerosols (Winker et al., 2003; Carn et al., 2007). CALIPSO completes 14.55 orbits per day with a 24.7° separation of longitude between each successive orbit at the equator. An analysis of the aerosol plume elevation observed by the different passes of CALIPSO between April 2 and April 11 is reported in Figure 3 as a function of their distance from La Réunion and their altitude.

Here, it is assumed that the observed aerosol plumes are mainly composed of sulfuric acid (H<sub>2</sub>SO<sub>4</sub>). The SO<sub>2</sub> in the plume is oxidized into H<sub>2</sub>SO<sub>4</sub> which then becomes particles through homogeneous nucleation or by deposition on pre-existing aerosols (Seinfeld and Pandis, 2006). This assumption is based primarily on the fact that there was no other major source of aerosols over the Indian Ocean during this period, except sea salt in the boundary layer.

Different CALIOP images are available on <http://www-calipso.larc.nasa.gov/products/>. In this paper, in order to select the volcanic aerosol plumes, the following CALIOP images are analysed in the geographic area corresponding to the plume observed with OMI (Fig. 4): (i) 532 nm Total Attenuated Backscattered, (ii) 1064 nm Total Attenuated Backscattered, (iii) Vertical Feature Mask, and (iv) Aerosol Subtype. The altitude of the observed plume is directly deduced from the "532 nm Total Attenuated Backscattered" picture. On April 3 and 4, CALIPSO's track observed Piton de la Fournaise's volcanic plumes west of La Réunion below 3000 m asl. Thus, there is no significant uplift of the SO<sub>2</sub> over La Réunion and the volcanic plume is still located in the lower troposphere level. From April 6, due to the very intense volcanic activity, the volcanic plumes cross the trade winds layer, reach the mid-troposphere and spread toward the east (see section 5). Indeed, on April 6, the CALIOP sensor detected three aerosol plumes close to La Réunion at 5500 m asl, 6500 m asl and 7500 m asl. On April 7, two aerosol

plumes are also observed. The LIDAR provides transects at 800 km (5500 m asl) and 1800 km (7300 m asl) east of La Réunion. These plumes probably correspond to those observed by OMI on April 6. SO<sub>2</sub> and sulfate aerosol lifetimes are longer in the upper troposphere compared to the lower atmosphere (Stevenson et al., 2003; Yang et al., 2009). Then we assume that the plumes observed by OMI on April 6 and 7 are also those observed by CALIOP at the east on April 8, 9, 10 and 11 at about 800 and 1100 km (6500 m asl and 10200 m asl), 1200 km (6300 m asl), 1000 km (9900 m asl) and 1200 km (3600 m asl) from La Réunion, respectively. This is consistent with the shape evolution of SO<sub>2</sub> plumes observed with OMI. Plume altitudes in the eastern Indian Ocean suggest that the transport of SO<sub>2</sub> continues in the days after the collapse of the crater. The field observations associated with cartography performed using OMI, allow a validation of the higher eastern plumes formed during three days (April 6, 7 and 8). In the western part of the Indian Ocean, between La Réunion and Madagascar, apart from April 9 and 11 (4200 m asl and 4400 m asl), plumes were never observed above 3100 m asl. The inversion layer was not crossed by these plumes that were formed by smaller volcanic activity.

## 4 Numerical simulation of the event

### 4.1 The MesoNH model

The mesoscale, non hydrostatic atmospheric model, MesoNH is used in this study. This model has been jointly developed by the Centre National de la Recherche Météorologique and the Laboratoire d'Aérodynamique (Lafont et al., 1998). MesoNH can be used to simulate small scale (LES type) to synoptic scale phenomena (horizontal resolution ranging from a few meters to several tens of kilometers), and it can be run in a two-way nested mode involving up to eight nesting stages. Different sets of parameterizations have been introduced for convection (Bechtold et al., 2001), cloud microphysics (Cohard and Pinty, 2000), turbulences (Bougeault and Lacarrere, 1989), biosphere-atmosphere thermodynamic exchanges (ISBA) (Noilhan and Mahfouf, 1996), urban-atmosphere interactions (Masson, 2000), lightning processes (Barthe et al., 2005), gaseous chemistry (Suhre et al., 1998; Tulet et al., 2003) and aerosols (Tulet et al., 2005; Grini et al., 2006).

For this study, the ReLACS chemical scheme (Crassier et al., 2000) has been used to represent the sulfur dioxide (SO<sub>2</sub>) oxidation and the formation of sulfuric acid (H<sub>2</sub>SO<sub>4</sub>).

### 4.2 Simulation configuration

The simulation started at 00 UTC on April 4, 2007, and ended at 00 UTC on April 11, 2007. The simulation domain is the same as the one used for the OMI in Section 3.1 (28.6°S and 10.9°S and 40.78°E and 71.22°E). The horizontal resolution of the model is 20 km which is comparable to

the OMI footprint size ( $13 \times 24 \text{ km}^2$ ). The vertical grid is composed of 60 vertical levels stretched up to an altitude of 24,000 m asl, with 30 levels between the surface and 1500 m asl. The initial and lateral boundary conditions are extracted from ECMWF analysis for the meteorology and from MOCAGE (Peuch et al., 1999) for gas chemistry.

### 4.3 Estimation of the day by day $\text{SO}_2$ release

The estimation of the gas emissions in the atmosphere during this eruption is a hard objective to reach due to the absence of any local rapid observing system of the gas in the vicinity of the volcano. To counterbalance this problem a top-down approach is adopted. Eckhardt et al. (2008) have developed a numerical top-down method to estimate the  $\text{SO}_2$  vertical profile by a volcanic eruption using satellite column measurement and inverse transport modeling. Although this method is robust and well adapted to the volcanic plume forecasting, we have chosen another way which is more basic, but more adapted to the particular situation of April 2007. Indeed, the strong variability in the lava flow between April 5 and April 7, have engendered strong variability of  $\text{SO}_2$  concentration in the plume. Moreover this discontinuity in the plume of  $\text{SO}_2$  (Fig. 2) was reinforced by meteorological processes such as scavenging and chemical transformation of  $\text{SO}_2$ . For these reasons the method used here to determine the  $\text{SO}_2$  profile above the eruption is based on an analysis of data, simulations tests, and the knowledge of the phenomenology of the eruption observed on the field. We proceed as follows:

- For each day, except April 6, the  $\text{SO}_2$  mass burden characteristics of the area around La Réunion are extracted from OMI. Due to the presence of clouds and the model resolution, the main difficulty is to estimate a characteristic mean value of  $\text{SO}_2$  suitable to be introduced into the model grid. Then, the estimated  $\text{SO}_2$  mass burden is converted into a homogeneous concentration of  $\text{SO}_2$  within the column of atmosphere located above the eruption (Table 1).

The top altitude of this column is estimated following two steps. First, the CALIPSO observations gives an estimate of the aerosol plume maximum altitude (Section 3.2). Second, a set of simulations is performed. Since the atmosphere is strongly vertically sheared in these regions (Baray et al., 1998; Clain et al., 2009) (Section 5), the lower and upper boundaries of the  $\text{SO}_2$  column over La Réunion is deduced.

- On April 6, the lava flux (and the  $\text{SO}_2$  release) is too variable to use the daily value from satellite. Moreover, as explained before, the presence of clouds prevents a correct estimate of  $\text{SO}_2$  by OMI over La Réunion. For these reasons, the  $\text{SO}_2$  concentration introduced in the La Réunion column for April 6, is estimated through a set of simulations, in order to fit to the plume observed on April 7. The global daily mass emitted in the sim-

ulation is adjusted to the total mass burden observed by OMI on April 7 (see section 6). The evolution of seismicity (Michon et al., 2007), associated with field observations, is also used to estimate the temporal variations of the emissions.

Furthermore, during the major eruptive period the  $\text{SO}_2$  plume is uplifted by convection and/or forced upward by the orography of La Réunion. This is due to the sensible heat flux (lava surface temperature  $\sim 1200^\circ\text{C}$ ) and the considerable latent heat flux generated by water evaporation when lava entered the ocean. In addition, the presence of steep relief (summit at 3070 m) can modify the trade winds flux around La Réunion (Lesouef et al., 2008), and can amplify the convection. These two processes are not reproduced by the model due to the horizontal resolution used in this study (20 km). The orography is smoothed, and the summit of La Réunion in the simulation is lowered to 500 m. For these reasons, the bottom of the  $\text{SO}_2$  column is chosen above the surface. Several simulations (not shown) have permitted us to adjust the altitude boundaries of the  $\text{SO}_2$  column introduced into the model. All data introduced into the model are reported in Table 1. At each time step of the model, a linear temporal interpolation is made between all the data of Table 1.

## 5 Evolution of the $\text{SO}_2$ plume over the Indian Ocean

### 5.1 $\text{SO}_2$ mass burden

Figure 5 represents the evolution of the  $\text{SO}_2$  mass burden simulated by MesoNH. This figure has to be compared to OMI observations (Fig. 2). The first period of April 4 and 5 shows that the plume is oriented toward the west in agreement with satellite observations. On April 5, the  $\text{SO}_2$  mass burden reaches 40 DU over La Réunion, which is the same order of magnitude as OMI observations.

On April 6, the model is able to reproduce the western and eastern branches of the  $\text{SO}_2$  plume, but the northern branch observed by OMI north of Mauritius is not wide enough in the simulation. The plume extending from La Réunion to Mauritius presents strong values of  $\text{SO}_2$  up to 70 DU. On April 7, the general shape of the  $\text{SO}_2$  distribution is retrieved. As for OMI observations, the western plume has reached Madagascar (Fig. 2.d). The main plume (50 DU) is oriented to the north, then turns to the east at  $17^\circ\text{S}$ . A large maximum at 40 DU is simulated north of Mauritius, which corresponds to the maximum of emission that occurred on April 6. As in the observations, the simulated  $\text{SO}_2$  plume reaches the eastern boundary of the domain. On April 8 and 9, the  $\text{SO}_2$  emission decreases strongly and the  $\text{SO}_2$  mass burden is moderate over La Réunion (4 to 10 DU). During this latter period, the simulation shows that the strong  $\text{SO}_2$  mass burden modeled on April 6 and 7 have been transported toward the south of Madagascar and to the north-east of the domain. An intense

tongue, with a maximum of 20 DU, extends over more than 1500 km on April 8.

## 5.2 April 7, vertical SO<sub>2</sub> distribution

To detail the vertical distribution of the SO<sub>2</sub> plume, Figure 6 displays the SO<sub>2</sub> concentration and the horizontal wind field at different altitudes on April 7, 2007 at 12 UTC. Close to the surface, the trade winds ( $6 \text{ m s}^{-1}$  above La Réunion) turns the SO<sub>2</sub> plume towards the west of La Réunion. The modeled surface SO<sub>2</sub> concentration is low. Our definition of the bottom altitude of the SO<sub>2</sub> column (Table 1) limits the plume extension to the west, as in OMI observations. Close to the eastern coast of Madagascar, the plume is more intense (20-40 ppbv) corresponding to the westerly plume of April 5. Due to the vertical wind shear over La Réunion, the plume is oriented to the north-west between 2 and 3 km asl, to the north at 4 km asl and to the north-east at 6 km asl (Fig. 5). As a consequence, the location of the SO<sub>2</sub> concentration maxima depends on the altitude. At 4 km asl, the maximum SO<sub>2</sub> concentration (100 ppbv) is located north of La Réunion. At 6 km asl, the plume is strengthened with a maximum concentration of more than 500 ppbv.

In the upper part of the plume (between 6 and 8 km asl), the plume is advected to a large distance from La Réunion by the south-west wind ( $10\text{-}15 \text{ m s}^{-1}$ ). At 8 km asl, the SO<sub>2</sub> maximum concentration decreases to 100 ppbv.

As for this particular day, the synoptic winds regime remains strongly sheared on the vertical during all the studied period. As explained in Section 4.2, a comparison between the plume observed by OMI and that given by different simulations, is used to initialize the altitude of the SO<sub>2</sub> plume above La Réunion.

## 5.3 Acid formation and deposition

This section is dedicated to an overview of the SO<sub>2</sub> and H<sub>2</sub>SO<sub>4</sub> dry deposition. Figure 7 shows the temporal integration of the SO<sub>2</sub> and H<sub>2</sub>SO<sub>4</sub> mass deposited on the surface between April 4 and April 10. Dry deposition occurs on the western part of the domain. Indeed, only this area is concerned by the significant surface concentration of SO<sub>2</sub> that is advected by the trade winds. In the simulation, about  $50 \text{ mg m}^{-2}$  of SO<sub>2</sub> is deposited in the vicinity of La Réunion, and  $15\text{-}20 \text{ mg m}^{-2}$  in a large tongue south east of Madagascar (Fig. 7.a). The order of magnitude of SO<sub>2</sub> mass deposition on land over Madagascar is in the range  $0.2\text{-}4 \text{ mg m}^{-2}$ .

For H<sub>2</sub>SO<sub>4</sub> (Fig. 7.b), the location of the mass deposition is quite different from SO<sub>2</sub>. Indeed, H<sub>2</sub>SO<sub>4</sub>, as a secondary species, is formed within the plume. As a consequence, the surface concentration of H<sub>2</sub>SO<sub>4</sub> is located in the western part of the domain (not shown), and a maximum of  $20 \text{ mg m}^{-2}$  of sulfuric acid deposit is simulated over the south-east of Madagascar.

The total dry deposition over the simulation domain for SO<sub>2</sub> and H<sub>2</sub>SO<sub>4</sub> is estimated to 27 kt and 21 kt, respectively.

## 6 Mass budget and estimated flux

### 6.1 Mass budget

This last section is devoted to the estimation of the mass budget of sulfur released into the atmosphere. Figure 8 shows the evolution of the integrated mass over the simulation domain for OMI (triangles, squares and circles), and for the simulation (solid lines). A volume calculation is performed on each "Digital SO<sub>2</sub> Model" with a threshold at 0.7 DU for TRL and 0.3 DU for TRM (see Section 3.1).

OMI observed a very pronounced evolution of SO<sub>2</sub> mass, from 10-20 kt on April 5, to 140 kt (TRM) and 286 kt (TRL) on April 7. One major problem comes from the strong deviation between TRM and TRL. To improve the OMI mass estimation, we assume that the center mass of the plume is located at 6000 m asl after the April 6. This altitude corresponds to the center of the SO<sub>2</sub> plume estimated above La Réunion, during the period of maximum degassing (see Table 1). The estimated OMI value, weighted between TRL and TRM, is represented on Figure 8 by squares. With this assumption, we estimate the maximum SO<sub>2</sub> mass at 190 kt on April 7. After April 7, the SO<sub>2</sub> mass decreases strongly and reaches 100 kt (68 kt for TRM and 155 kt for TRL) on April 8. Then, the SO<sub>2</sub> mass decreases slowly. On April 10, the SO<sub>2</sub> mass reaches 41 kt (TRM) and 77 kt (TRL).

The black solid line in Figure 8 gives the evolution of an inert gas for which no chemical transformation or deposition can occur. The maximum of this curve reaches 219 kt on April 7. The decrease in the simulated mass after midday on April 7 corresponds to the mass escape through the domain boundary. It can be estimated 50 kt, but cannot explain the 210 kt and 110 kt decrease during the period, observed by OMI upon TRL or TRM, respectively.

The evolution of the simulated SO<sub>2</sub> mass (solid blue line) differs from the tracer by two integrative processes: the chemical oxidation into H<sub>2</sub>SO<sub>4</sub> and the dry deposition to the surface. Thus, the evolution of the SO<sub>2</sub> mass reaches a maximum at 200 kt on April 8, and then decreases to 140 kt at the end of the simulation. In parallel, the H<sub>2</sub>SO<sub>4</sub> (solid red line) gradually increases to 40 kt on April 10. The oscillation in the production of H<sub>2</sub>SO<sub>4</sub> corresponds to the balance between the oxidation of SO<sub>2</sub>, which is efficient during the day, and the loss by dry deposition or the escape through the domain boundaries. Nevertheless, the evolution of the SO<sub>2</sub> mass that integrates the loss at the surface, the oxidation and the escape out of the domain still overestimates by at least 60 kt the mass observed by OMI at the end of the simulated period.

To compare with TRM and TRL, two other curves filter out every column of SO<sub>2</sub> lower than 0.3 DU (green solid line) and 0.7 DU (yellow solid line). These new curves reproduce the increase of the integrated mass between April 4 and April 7, and reaches the maximum estimated value of 190 kt on April 7 (Figure 8). The decrease of mass reaches 120 kt at the end of the simulation, which represents an overestimation ranging between 40 and 80 kt compared to OMI values. Three hypotheses related to clouds presence can be given to explain these differences. First, cloud prevent the correct observation of SO<sub>2</sub>: in cloudy regions, the mass observed by OMI is globally underestimated in agreement with Carn et al. (2008). This is clear for April 6 where the weather over La Réunion and Mauritius is cloudy (Figure 2.c). This is also visible through the discontinuity in the observed plume on April 7 (Figure 2.d). Second, the presence of clouds implies the possible presence of precipitation that can scavenge the SO<sub>2</sub>. Comparing the simulated and the observed SO<sub>2</sub> in Madagascar region on April 8 and 9, (Figures 2 and 5), we can assume that a non-negligible amount of SO<sub>2</sub> is washed out. Third, the model does not integrate the aqueous chemistry that transforms the SO<sub>2</sub> into H<sub>2</sub>SO<sub>4</sub> in cloud droplets. So, in cloudy areas, the formation of H<sub>2</sub>SO<sub>4</sub> is underestimated by the model which could explain part of the modeled SO<sub>2</sub> overestimation during the last period.

In addition the dispersion of SO<sub>2</sub> over time will decrease the column amounts below the OMI detection limits, particularly at the fringes of the volcanic plume. So, less SO<sub>2</sub> will be measured from space, even though the SO<sub>2</sub> is still present. The model does not suffer from this finite sensitivity.

## 6.2 Estimation of the SO<sub>2</sub> flux

To estimate the SO<sub>2</sub> release into the atmosphere, the SO<sub>2</sub> concentration introduced in the model is maintained in the column above Piton de la Fournaise (Section 4.3). Then the emission at the surface must compensate for the mass of SO<sub>2</sub> advected out of the column located above the eruption. It can be formulated using the initial  $F(0)$  and the iterative  $F(t)$  fluxes (in  $\mu\text{g m}^{-2} \text{s}^{-1}$ ) defined as:

$$F(0) = \frac{M_{SO_2}}{M_{air} \Delta t} \sum_{k=bot}^{top} \rho_k [SO_2]_k \Delta Z_k$$

and

$$F(t) = \frac{M_{SO_2}}{M_{air} \Delta X \Delta Y} \sum_{k=bot}^{top} \rho_k [SO_2]_k \Delta Z_k (u_k \Delta Y + v_k \Delta X - u_k v_k \Delta t)$$

where  $[SO_2]_k$  is the SO<sub>2</sub> concentration at level  $k$  (ppbv),  $\Delta t$  the time step of the model (s),  $\rho_k$  the air density ( $\text{kg m}^{-3}$ ),  $u_k$  and  $v_k$  the zonal and meridian wind ( $\text{m s}^{-1}$ ), and  $\Delta X$ ,  $\Delta Y$ ,  $\Delta Z_k$  the grid sizes of the domain along the west-east and south-north axes, and the altitude (m). The index  $k$  represents the altitude level of the model.  $M_{SO_2}$  and  $M_{air}$  ( $\text{kg mol}^{-1}$ ) represent the molecular weight for SO<sub>2</sub> and air, respectively.

Using this formulation, the SO<sub>2</sub> emission estimated by the model is shown in Figure 9. The model retrieves a strong evolution of the emission on April 6 reaching  $1800 \text{ kg s}^{-1}$  over a surface of  $20 \times 20 \text{ km}^2$  which corresponds to the surface of the horizontal grid of the model. This strong increase is related to the increase of SO<sub>2</sub> concentration introduced into the eruptive column on April 6 (Table 1). Note that this evolution of the emission is not smoothed due to the variability of the horizontal wind. A day by day mass budget is also reported in Figure 9. The analytic computation of the mass emission during the main days of the eruption is 12 kt, 43 kt and 125 kt for April 5, April 6 and April 7, respectively. The total emission given by the model during the period is 231 kt of SO<sub>2</sub>, and 218 kt until April 8. This latter value is comparable to the maximum mass of the tracer simulated (219 kt). These computations integrate many sources of possible errors from the model (winds and depositions), and from the SO<sub>2</sub> mass retrieved by OMI (algorithm, altitude of the plume on April 7). Then, these estimations must be taken with caution and as an order of magnitude.

## 7 Conclusions

This original study has two objectives. Firstly, it is devoted to analysis at the synoptic scale of the becoming of SO<sub>2</sub> released into the atmosphere by the eruption of the Piton de la Fournaise volcano. OMI observations show a strong variability in the mass of SO<sub>2</sub> over the domain. The first question is to understand which physical processes are able to generate this strong variability. The simulation of the event using the mesoscale model MesoNH gave some answers. Several numerical three-dimensional calibration runs of the model were performed using the OMI and CALIPSO observations, and through the comparison of the large scale plumes provided by MesoNH and OMI. The final result gives a correct representation of the main plumes by the model during the period April 4-9, 2007. The model estimates that 231 kt of SO<sub>2</sub> are emitted into the atmosphere during the period. The numerical simulations also emphasizes the becoming of the volcanic sulfur. During this event, the simulation estimates 60 kt of SO<sub>2</sub> are oxidized into H<sub>2</sub>SO<sub>4</sub>, of which 21 kt are lost at the surface by dry deposition. A sink of 27 kt of SO<sub>2</sub> by dry deposition must be added to the SO<sub>2</sub> budget. By differencing with the total amount of SO<sub>2</sub> present in the atmosphere at the end of the simulation (140 kt), less than 4 kt of SO<sub>2</sub> are estimated to have escaped through the domain boundaries.

Nevertheless, these mass budgets have to be taken with caution. Due to the resolution of the model that cannot correctly represents the cloud microphysics, the aqueous process of scavenging by rain and the SO<sub>2</sub> transformation into acid in the cloud droplets are not taken into account in this study. As a consequence, the total deposition at the

surface and the amount of acid formed is underestimated. Thus, the estimation of the SO<sub>2</sub> released into the atmosphere on April 6, where precipitations are present, is also probably underestimated. For these reasons, the values of SO<sub>2</sub> mass and the chemical transformation given by the model have to be taken as a low limit of the reality.

The second objective of this study is to retrieve the SO<sub>2</sub> emission during the eruption by a top-down approach. It consists of maintaining an SO<sub>2</sub> concentration in a column located above Piton de la Fournaise. The estimation of the SO<sub>2</sub> surface flux is then based on the fact that the emission flux is equal to the exportation of SO<sub>2</sub> out of the eruptive column. Using this method a strong variability of SO<sub>2</sub> emission is retrieved, in particular with a peak on April 6 reaching 1800 kg s<sup>-1</sup> on the surface model grid.

One important perspective of this study is to introduce this surface flux estimate into high resolution simulations. Through high resolution studies, it will be possible to reproduce the local convection, the precipitation and the aqueous chemical transformation of gas that formed acid rains. These topics that link the air pollution and their consequences on human health and ecosystems will constitute the future plans for this work.

*Acknowledgements.* We greatly acknowledge F. Caillé and R. Delmas for providing the pictures of the 2007 eruption. We thank L. Michon and N. Krotkov for their relevant comments. We also would like to thank the MesoNH assistance team for their support and availability, C. Barthe and J. Kemp for improvement of the English.

## References

- Afe, O., Richter, A., Sierk, B., Wittrock, F., and Burrows, J.: BrO Emission from Volcanoes - a Survey using GOME and SCIAMACHY Measurements, *Geophysical Res. Lett.*, 31, 124113, doi:10.1029/2004GL020994, 2004.
- Arellano, S., Hall, M., Samaniego, P., LePennec, J., Ruiz, A., Molina, I., and Yepes, H.: Degassing patterns of Tungurahua volcano (Ecuador) during the 1999-2006 eruptive period, inferred from remote spectroscopic measurements of SO<sub>2</sub> emissions., *J. Volcanol. Geotherm. Res.*, 176, 151–162, doi:10.1016/j.jvolgeores.2008.07.007, 2008.
- Baray, J., Ancellet, G., Taupin, F., Bessafi, M., Baldy, S., and Keckhut, P.: Subtropical tropopause break as a possible stratospheric source of ozone in the tropical troposphere, *J. Atmos. Solar-Terr. Phys.*, 60, 27–36, 1998.
- Barthe, C., Molini, G., and Pinty, J.: Description and first results of an explicit electrical scheme in a 3D Cloud Resolving Model, *Atmos. Res.*, 76, Issues 1-4, 95–113, 2005.
- Bechtold, P., Bazile, E., Guichard, F., Mascart, P., and Richard, E.: A mass-flux convection scheme for regional and global models, *Quart. J. Roy. Meteor. Soc.*, 127, 869–886, 2001.
- Bhugwant, C., Siéja, B., Bessafi, M., Staudacher, T., and Ecomier, J.: Atmospheric sulfur dioxide measurements during the 2005 and 2007 eruptions of the Piton de la Fournaise volcano: Implications for human health and environmental changes., *J. Volcanol. Geotherm. Res.*, 184, 208–224, doi:10.1016/j.jvolgeores.2009.04.012, 2008.
- Bougeault, P. and Lacarrere, P.: Parametrization of orography-induced turbulence in a meso-beta model, *Mon. Wea. Rev.*, 117, 1872–1890, 1989.
- Carn, S., Krotkov, N., Yang, K., Hoff, R., Prata, A., Krueger, A., Loughlin, S., and Levelt, P.: Extended observations of volcanic SO<sub>2</sub> and sulfate aerosol in the stratosphere, *Atmos. Chem. Phys. Disc.*, 7, 2857–2871, 2007.
- Carn, S., Krueger, A., Arellano, S., Krotkov, N., and Yang, K.: Ecuadorian volcanic degassing from space., *J. Volcanol. Geotherm. Res.*, 176, 141–150, doi:10.1016/j.jvolgeores.2008.01.029, 2008.
- Clain, G., Baray, J., Delmas, R., Diab, R., de Bellevue, J. L., Keckhut, P., Posny, F., Metzger, J., and Cammas, J.: Tropospheric ozone climatology at two Southern Hemisphere tropical/subtropical sites ( Reunion Island and Irene, South Africa) from ozonesondes, LIDAR and in-situ aircraft measurements, *Atmos. Chem. Phys.*, 9, 1723–1734, 2009.
- Cohard, J. and Pinty, J.: A comprehensive two-moment warm microphysical bulk scheme . II : 2D experiments with a non hydrostatic model, *Quart. J. Roy. Meteor. Soc.*, 126, 1843–1859, 2000.
- Coppola, D., Piscopo, D., Staudacher, T., and Cigolini, C.: Lava discharge rate and effusive pattern at Piton de la Fournaise from MODIS data., *J. Volcanol. Geotherm. Res.*, 184, 174–192, doi:10.1016/j.jvolgeores.2008.11.031, 2009.
- Crassier, V., Suhre, K., Tulet, P., and Rosset, R.: Development of a reduced chemical scheme for use in mesoscale meteorological models, *Atmos. Environ.*, 34, 2633–2644, 2000.
- Delmelle, P., Stix, J., Baxter, P., Garcia-Alvarez, J., and Barquero, J.: Atmospheric dispersion, environmental effects and potential health hazard associated with the low-altitude gas plume of Masaya volcano, Nicaragua., *Earth and Environmental Science*, pp. 423–434, 10.1007/s00445-002-0221-6, 2002.
- Deroussi, S., Diamant, M., Feret, J., Nebut, T., and Staudacher, T.: Localization of cavities in a thick lava flow by microgravimetry., *J. Volcanol. Geotherm. Res.*, 184, 193–198, doi:10.1016/j.jvolgeores.2008.10.002, 2009.
- Diab, R., Thompson, A., Mari, K., Ramsay, L., and Coetzee, G.: Tropospheric ozone climatology over Irene, South Africa, From 1990 to 1994 and 1998 to 2002., *J. Geophys. Res.*, 109, D20301, doi:10.1029/2004JD004793, 2004.
- Eckhardt, S., Prata, A., Seibert, P., Stebel, K., and Stohl, A.: Estimation of the vertical profile of sulfur dioxide injection into the atmosphere by a volcanic eruption using satellite column measurements and inverse transport modeling, *Atmos. Chem. Phys.*, 8, 3881–3897, 2008.
- Edmonds, M., Oppenheimer, C., Pyle, D., and Herd, R.: Rainwater and ash leachate analysis as proxies for plume chemistry at Soufrière Hills Volcano, Monserrat, in: *Volcanic Degassing*, edited by C. Oppenheimer, D. P. and Barclay, J., vol. 213, pp. 203–218, Geophysical Society, London Special Publication, 2003.
- Georgoulias, A., Balis, D., Koukouli, M., Meleti, C., Bais, A., and Zerefos, C.: A study of the total atmospheric sulfur dioxide load using ground-based measurements and the satellite derived Sulfur Dioxide Index., *Atmos. Environ.*, 43(9), 1693–1701,

- doi:10.1016/j.atmosenv.2008.12.012, 2009.
- Grini, A., Tulet, P., and Gomes, L.: Dusty weather forecast using the MesoNH atmospheric model., *J. Geophys. Res.*, 111, doi:10.1029/2005JD007007, 2006.
- Hoffman, D.: Perturbations to the global atmosphere associated with the El Chichón volcanic eruption of 1982, *Rev. Geophys.*, 25, 743–759, 1987.
- Hoffman, D. J., Rosen, J., and Gringel, W.: Delayed production of sulfuric acid condensation nuclei in the polar stratosphere from El Chichon volcanic vapors., *J. Geophys. Res.*, 90, 2341–2354, 1985.
- Khokhar, M., Frankenberg, C., VanRoosendael, M., Beirle, S., Kuhl, S., Richter, A., Platt, U., and Wagner, T.: Satellite observations of atmospheric SO<sub>2</sub> from volcanic eruptions during the time-period of 1996–2002., *Advances in Space Research*, 36(5), 879–887, 2005.
- Krotkov, N., Carn, S., Krueger, A., Bhartia, P., and Yang, K.: Band residual difference algorithm for retrieval of SO<sub>2</sub> from the Aura Ozone Monitoring Instrument (OMI)., *IEEE Trans. Geosci. Remote Sens.*, 44 (5), 1259–1266, 2006.
- Krotkov, N., McClure, B., Dickerson, R., Carn, S., Li, C., Bhartia, P., Yang, K., Krueger, A., Li, Z., Levelt, P., Chen, H., Wang, P., and Lu, D.: Validation of SO<sub>2</sub> retrievals from the Ozone Monitoring Instrument over NE China, *J. Geophys. Res.*, 113, D16S40, doi:10.1029/2007JD008818, 2008.
- Krueger, A., Walter, L., Bhartia, P., Schnetzler, C., Krotkov, N., Sprod, I., and Bluth, G.: Volcanic sulfur dioxide measurements from the total ozone mapping spectrometer instruments., *J. Geophys. Res.*, 100(D7), 14,057–14,076, 1995.
- Kulmala, M., Laaksonen, A., and Pirjola, L.: Parametrization for sulfuric acid / water nucleation rates, *J. Geophys. Res.*, 103, D7, 8301–8307, 1998.
- Lafore, J., Stein, J., Asencio, N., Bougeault, P., Ducrocq, V., Duron, J., Fischer, C., Hereil, P., Mascart, P., Pinty, V. M. J., Redelsperger, J., Richard, E., and de Arellano, J. V.-G.: The Meso-NH atmospheric simulation system. Part I: adiabatic formulation and control simulations, *Ann. Geophys.*, 16, 90–109, 1998.
- Lenat, J. and Bachelery, P.: Dynamics of Magma Transfer at Piton de La Fournaise Volcano (Réunion Island, Indian Ocean)., in: *Earth Evolution Sciences - Special Issue Modeling of Volcanic Processes*, edited by Chi-Yu, K. and R., S., pp. 57–72, Friedr. Vieweg and Sohn, Braunschweig/Wiesbaden, 1987.
- Lesouef, D., Gheusi, F., and R.Delmas: Etude numérique des circulations locales á la Réunion : application aux transports de polluants, *La Mét'eorologie*, 62, 32–38, 2008.
- Martin, R., Mather, T., Pyle, D., Power, M., Allen, A., Aiuppa, A., Horwell, C., and Ward, E.: Composition-resolved size distributions of volcanic aerosols in the Mt. Etna plumes, *J. Geophys. Res.*, 113, D17211, doi:10.1029/2007JD009648, 2008.
- Masson, V.: A physically-based scheme for the urban energy balance in atmospheric models, *Boundary-Layer Meteorology*, 94, 357–397, 2000.
- Mather, T., Pyle, D., and Oppenheimer, C.: Tropospheric Volcanic Aerosol, *Geophys. Mono.*, 139, 189–212, doi:10.1029/139GM12, 2005.
- McCormick, M., Thomason, L., and Trepte, C.: Atmospheric effects of the Mt-Pinatubo eruption, *Nature*, 373, 399–404, 1995.
- Michon, L., Staudacher, T., Ferrazzini, V., Bachelery, P., and Marti, J.: April 2007 collapse of Piton de la Fournaise: a new example of caldera formation, *Geophysical Res. Let.*, 31, 121301, doi:10.1029/2007GL031248, 2007.
- Michon, L., Villeneuve, N., Catry, T., and Merle, O.: How summit calderas collapse on basaltic volcanoes: New insights from the April 2007 caldera collapse of Piton de la Fournaise volcano., *J. Volcanol. Geotherm. Res.*, 184, 138–151, doi:10.1016/j.jvolgeores.2008.11.003, 2009.
- Noilhan, J. and Mahfouf, J.: The ISBA land surface parameterization scheme., *Global and Plan. Change*, 13, 145–159, 1996.
- Oppenheimer, C., Pyle, D., and Barclay, J.: *Volcanic degassing*, vol. 213, *Geophysical Society, London Special Publication*, 2003.
- Peltier, A., Staudacher, T., Bachelery, P., and Cayol, V.: Formation of the April 2007 caldera collapse at Piton de La Fournaise volcano: Insights from GPS data., *Volcanol. Geotherm. Res.*, 184, 152–163, doi:10.1016/j.jvolgeores.2008.09.009, 2009.
- Penner, J., Andreae, M., Annegarn, H., Barrie, L., Feichter, J., Hegg, D., Jayaraman, A., Leaitch, R., Murphy, D., Nganga, J., and Pitari, G.: Aerosols, their direct and indirect effects, *Climate Change: The scientific basis*, pp. 289–349, edited by J.T. Houghton, Y. Ding, D.J. Griggs, M. Noguer, P.J. Van der Linden, X. Dai, K. Maskell and C.A. Johnson, Cambridge University Press, UK, 2001.
- Peuch, V., Amodei, M., Barthet, T., Cathala, M., Josse, B., Michou, M., and Simon, P.: MOCAGE : Modèle de Chimie Atmosphérique á Grande Echelle, AMA, CNRM, Toulouse, France., 1999.
- Pollack, J., Toon, O., Danielsen, E., Hofmann, D., and Rosen, J.: The El Chichón volcanic cloud - an introduction, *Geophysical Res. Let.*, 10, 989–992, 1983.
- Robock, A.: Pinatubo eruption - The climatic aftermath, *Science*, 295, 1242–1244, 2002.
- SaintAnge, S.: La sdimentation volcanoclastique en contexte de point chaud (ile de La Réunion, Océan Indien), Thesis, University of La Reunion, France, 2009.
- Seifert, P., Gross, S., Ansmann, A., Freudenthaler, V., Hiebsch, A., Schmidt, J., Schnell, F., Tesche, M., and Wiegner, M.: Heterogeneous ice nucleation in the ash plume of Eyjafjöll observed at two central-European EARLINET lidar sites., in: *The 13th Conference on Cloud Physics / 13th Conference on atmospheric Radiation (28 June - 2 July 2010)*, AMS, Portland, USA, 2010.
- Seinfeld, J. and Pandis, S.: *Atmospheric Chemistry and Physics*, Second edition, Wiley interscience pub, 2006.
- Staudacher, T., Ferrazzini, V., Peltier, A., Kowalski, P., Boissier, P., Catherine, P., Lauret, F., and Massin, F.: The April 2007 eruption and the Dolomieu crater collapse, two major events at Piton de la Fournaise (La Runion Island, Indian Ocean)., *J. Volcanol. Geotherm. Res.*, 184, 126–137, doi:10.1016/j.jvolgeores.2008.11.005, 2009.
- Stevenson, D., Johnson, C., Collins, W., and Derwent, R.: The tropospheric sulphur cycle and the role of volcanic SO<sub>2</sub>, *Geological Society special publication*, 213, 295–305, 2003.
- Suhre, K., Mari, C., Bates, T., Johnson, J., Rosset, R., Wang, Q., Bandy, A., Blake, D., Businger, S., Eisels, F., Huebert, B., Kok, G., Mauldin, R. I., Prévôt, A., Schillawski, R., Tanner, D., and Thornton, D.: Physico-chemical modeling of the First Aerosol Characterization Experiment (ACE 1) Lagrangian B, 1. A moving column approach, *J. Geophys. Res.*, 103, 16433–16455, 1998.
- Sutton, A., Elias, T., Gerlach, T., and Stokes, J.: Implications for

- eruptive processes by sulphur dioxide emissions from Kilauea Volcano, Hawaii, *J. Volcanol. Geotherm. Res.*, 108, 283–302 and 423–434, 2001.
- Thomas, H., Watson, I., Carn, C. K. S., and Murray, S.: A multi-sensor comparison of sulphur dioxide emissions from the 2005 eruption of Sierra Negra volcano, Galapagos Islands, *Remote Sensing of Environment*, 113, 1331–1342, doi:10.1016/j.rse.2009.02.019, 2009.
- Tulet, P., Crassier, V., Solmon, F., Guedalia, D., and Rosset, R.: Description of the MESOScale NonHydrostatic Chemistry model and application to a transboundary pollution episode between northern France and southern England, *J. Geophys. Res.*, 108, D1, 4021, doi:10.1029/2000JD000301, 2003.
- Tulet, P., Crassier, V., Cousin, F., Shure, K., and Rosset, R.: ORILAM, A three moment lognormal aerosol scheme for mesoscale atmospheric model. On-line coupling into the MesoNH-C model and validation on the ESCOMPTE campaign, *J. Geophys. Res.*, 110, D18201, doi:10.1029/2004JD005716, 2005.
- Winker, D. M., Pelon, J., and McCormick, M.: The CALIPSO mission: Spaceborne lidar for observation of aerosols and clouds, *Symposium on Remote Sensing of the Atmosphere, Environment and Space, Hangzhou, China, 23-27 October 2002.*, 4893, 1–11, 2003.
- Yang, K., Krotkov, N., Krueger, A., Carn, S., Bhartia, P., and Lev-elt, J.: Retrieval of large volcanic  $SO_2$  columns from the Aura Ozone Monitoring Instrument (OMI): comparisons and limitations., *J. Geophys. Res.*, 112, doi:10.1029/2007JD008825, 2007.
- Yang, K., Liu, X., Krotkov, N., Krueger, A., and Carn, S.: Estimating the altitude of volcanic sulfur dioxide plumes from space borne hyper-spectral UV measurements., *Geophysical Res. Lett.*, 36, 1–6, 110803, doi:10.1029/2009GL038025, 2009.



**Fig. 1.** a, b and d: Lava flow on Le Grand Brûlé area near the Piton Tremblet crater on April 5, 6 and 8, 2007, respectively. Copyright F. Caillé. (c): Three different plumes over the Piton de la Fournaise during the collapse of the Dolomieu crater on April 6, 2007. Copyright R. Delmas.

Day of April, 2007	4	5	5	6	6	7	8	9	10
Hours (UTC)	11	11	22	9	15	5	11	10	11
Bottom (m asl)	surface	500	3500	4000	4000	3000	500	surface	surface
Top (m asl)	2000	5000	6000	9000	9000	8000	4000	2500	2500
SO <sub>2</sub> (Du)	3	30	70	100	100	40	4.5	3	3

**Table 1.** Evolution of the column size and the SO<sub>2</sub> concentration introduced into the model over La Réunion between April 4 and April 10, 2007.

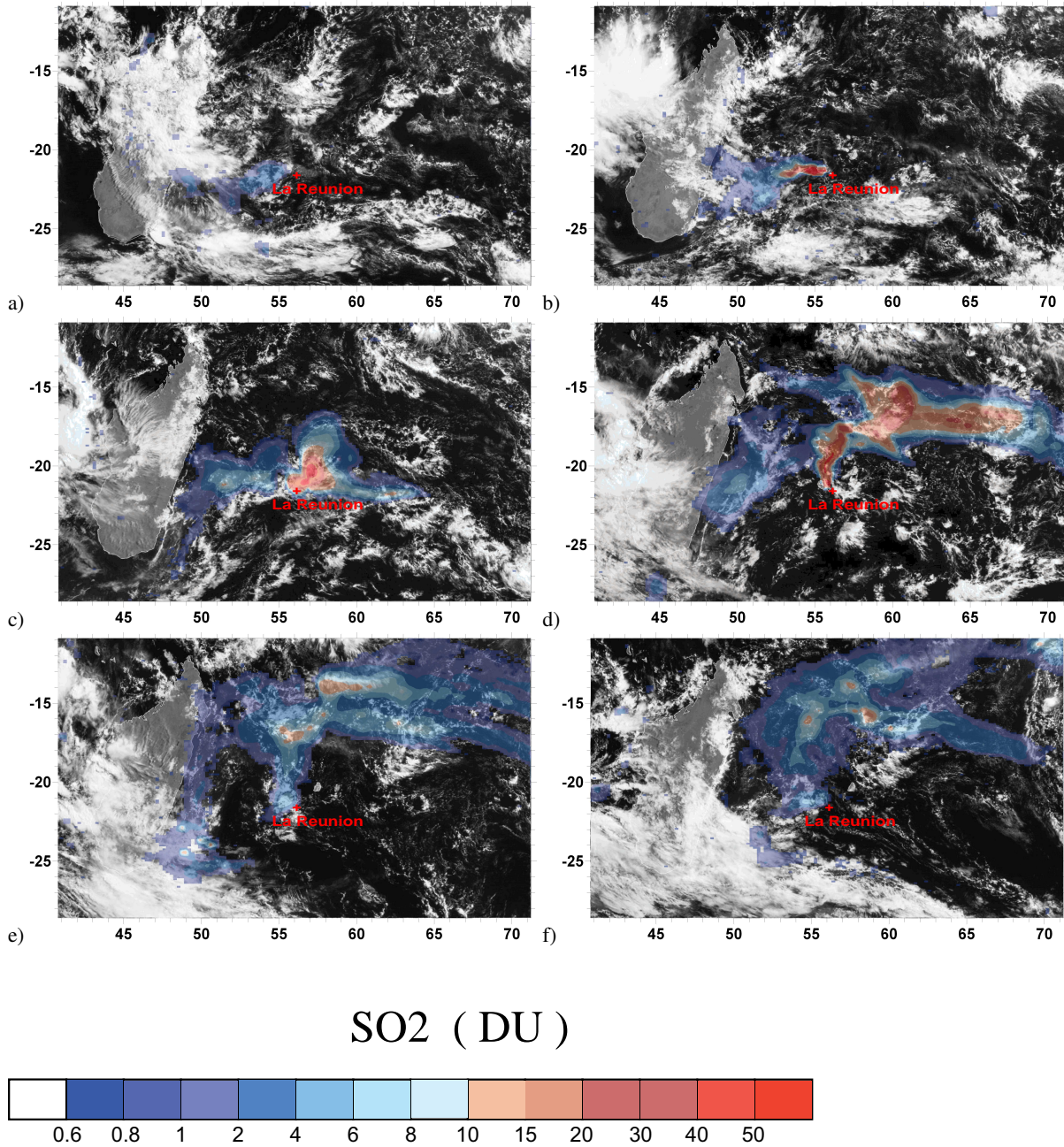


**Fig. 2.** SO<sub>2</sub> mass burden (Dobson Units) measured by OMI superimposed on the Meteosat visible channel, on April 4 at 11 UTC (a), April 5 at 10 UTC (b), April 6 at 11 UTC (c), April 7 at 10 UTC (d), April 8 at 11 UTC (e) and April 9 at 10 UTC (f).

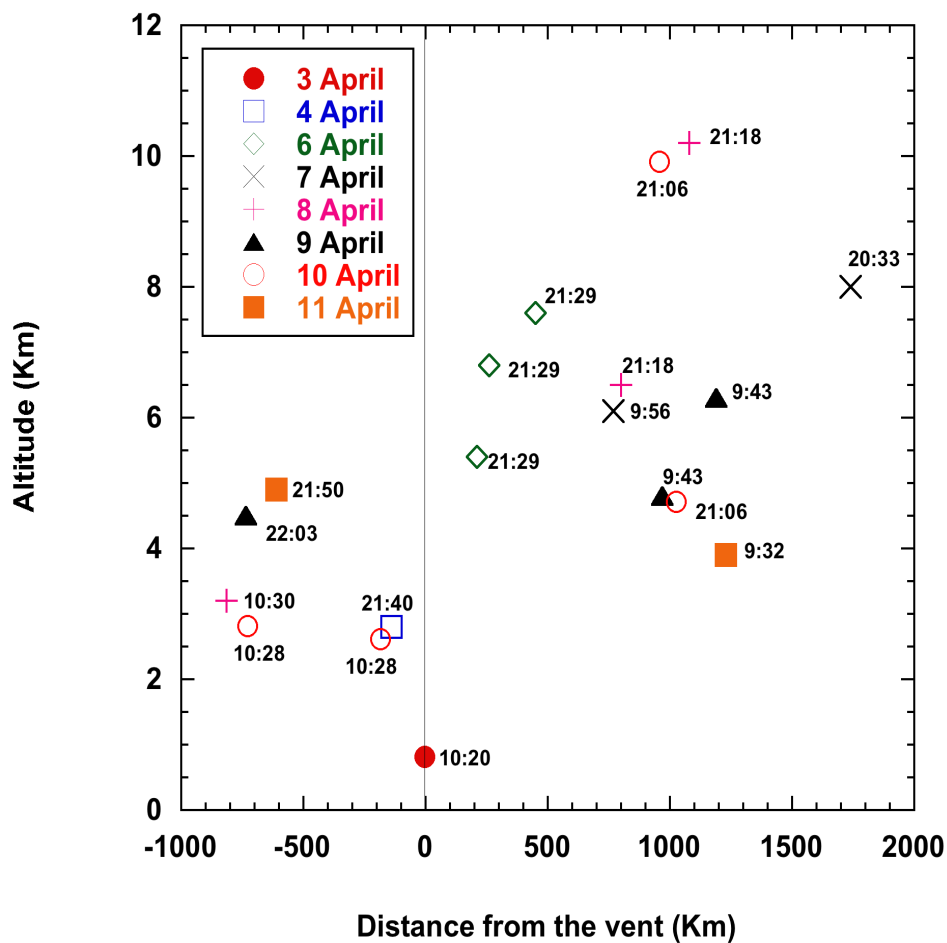


**Fig. 3.** Altitude and distance from La Réunion of the aerosols plumes observed by the CALIOP sensor on the CALIPSO satellite from April 3 to April 11, 2007 at different times (plotted). Negative abscissa values correspond to the west, and positive values to the east.

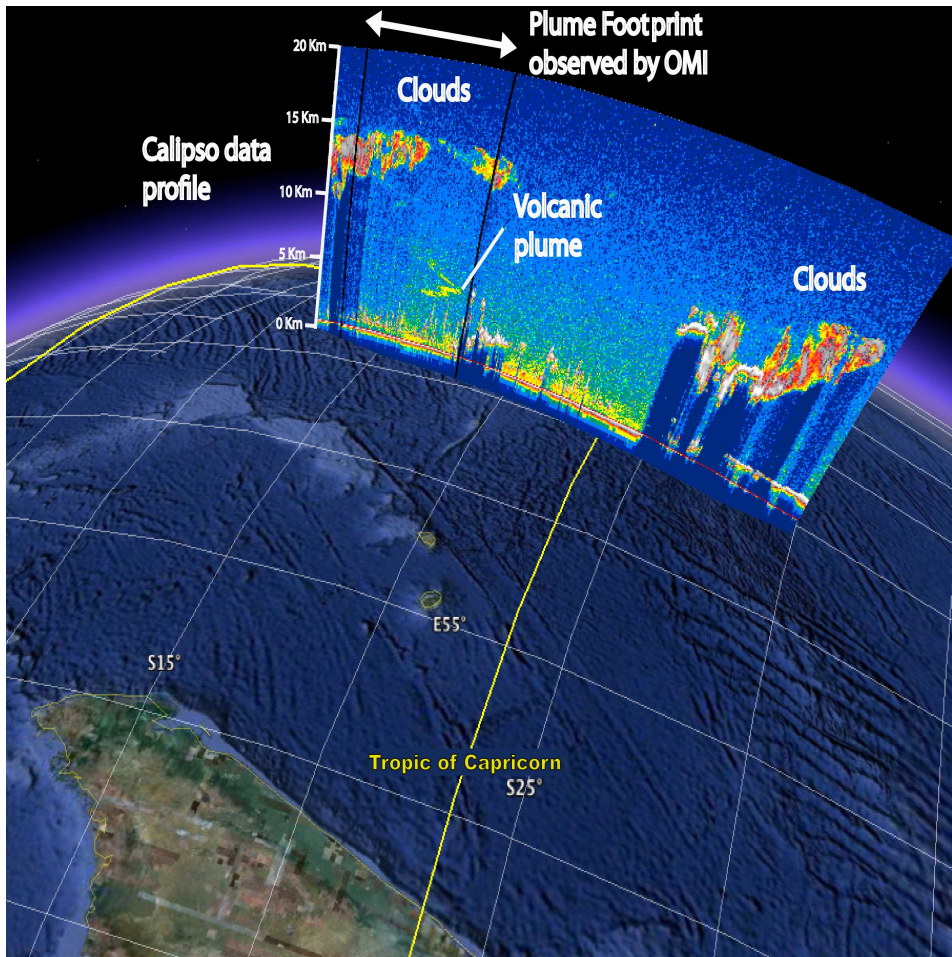


**Fig. 4.** Vertical CALIOP profile (532 nm Total Attenuated Backscattered) over Indian Ocean showing the volcanic Plume on April 8, 2007 at 21 UTC (data obtained and modified from <http://www-calipso.larc.nasa.gov/products> and Google Earth).

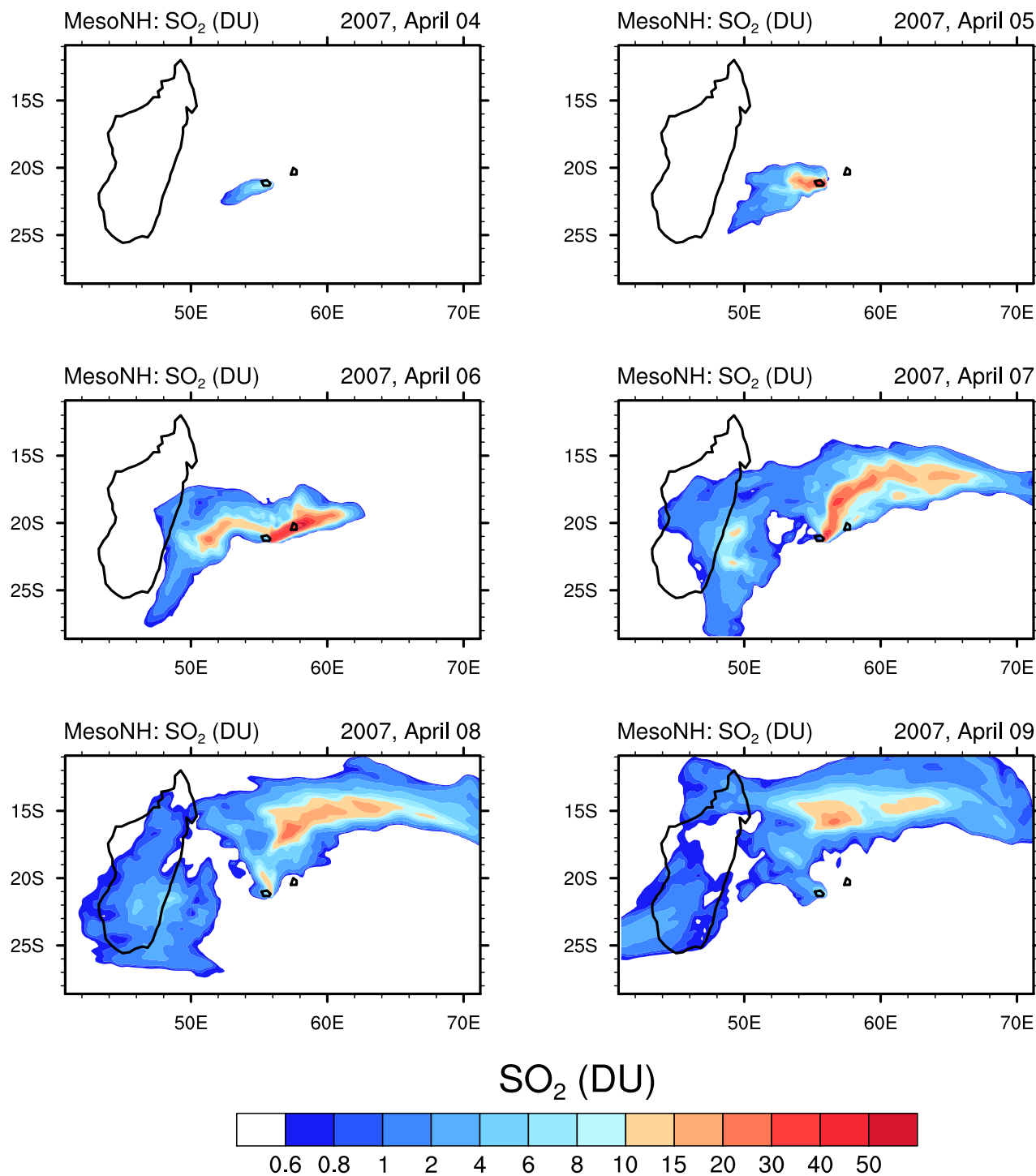


**Fig. 5.** Evolution of SO<sub>2</sub> mass burden simulated by MesoNH at 12 UTC for the period April 4-9, 2007.

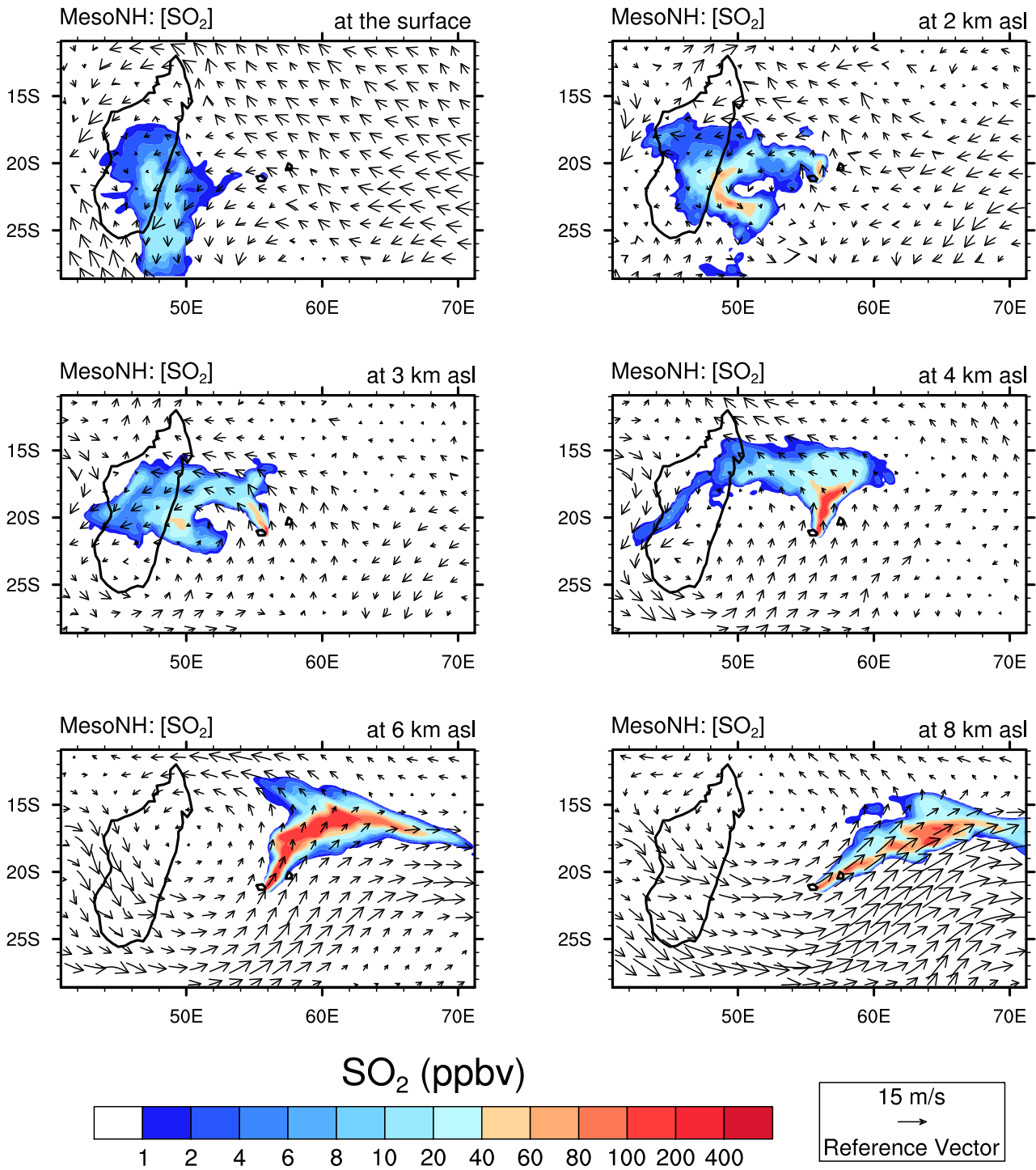


**Fig. 6.** Concentration of  $\text{SO}_2$  (ppbv) and horizontal wind vector (reference at the bottom right) simulated by MesonH on April 7, 2007, at different levels (surface, 2 km asl, 3 km asl, 4 km asl, 6 km asl and 8 km asl).

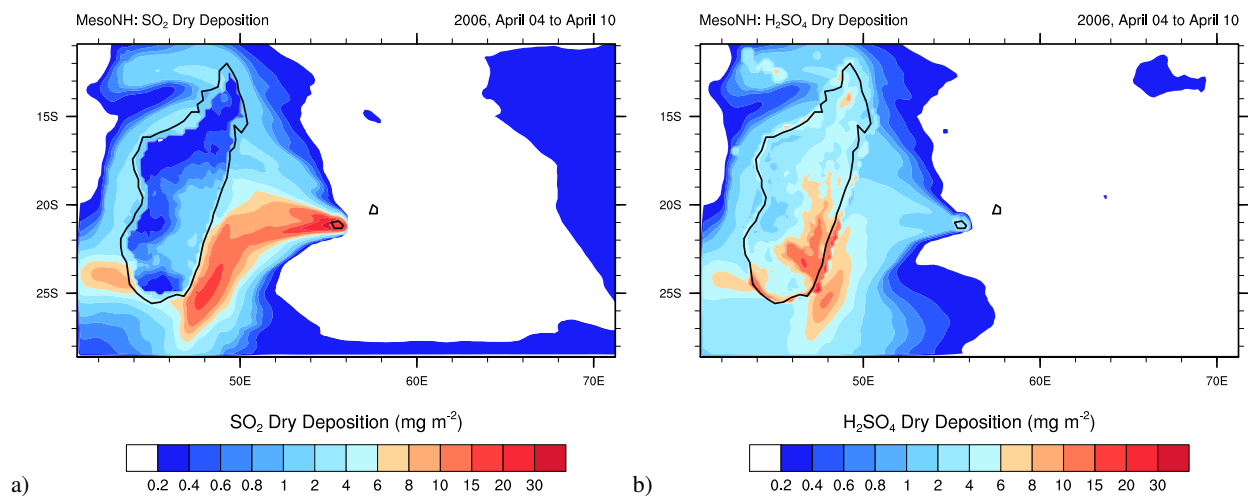


**Fig. 7.** Surface dry deposition of SO<sub>2</sub> (a) and H<sub>2</sub>SO<sub>4</sub> (b) ( $mg.m^{-2}$ ), simulated by MesoNH between April 4 and April 11, 2007.

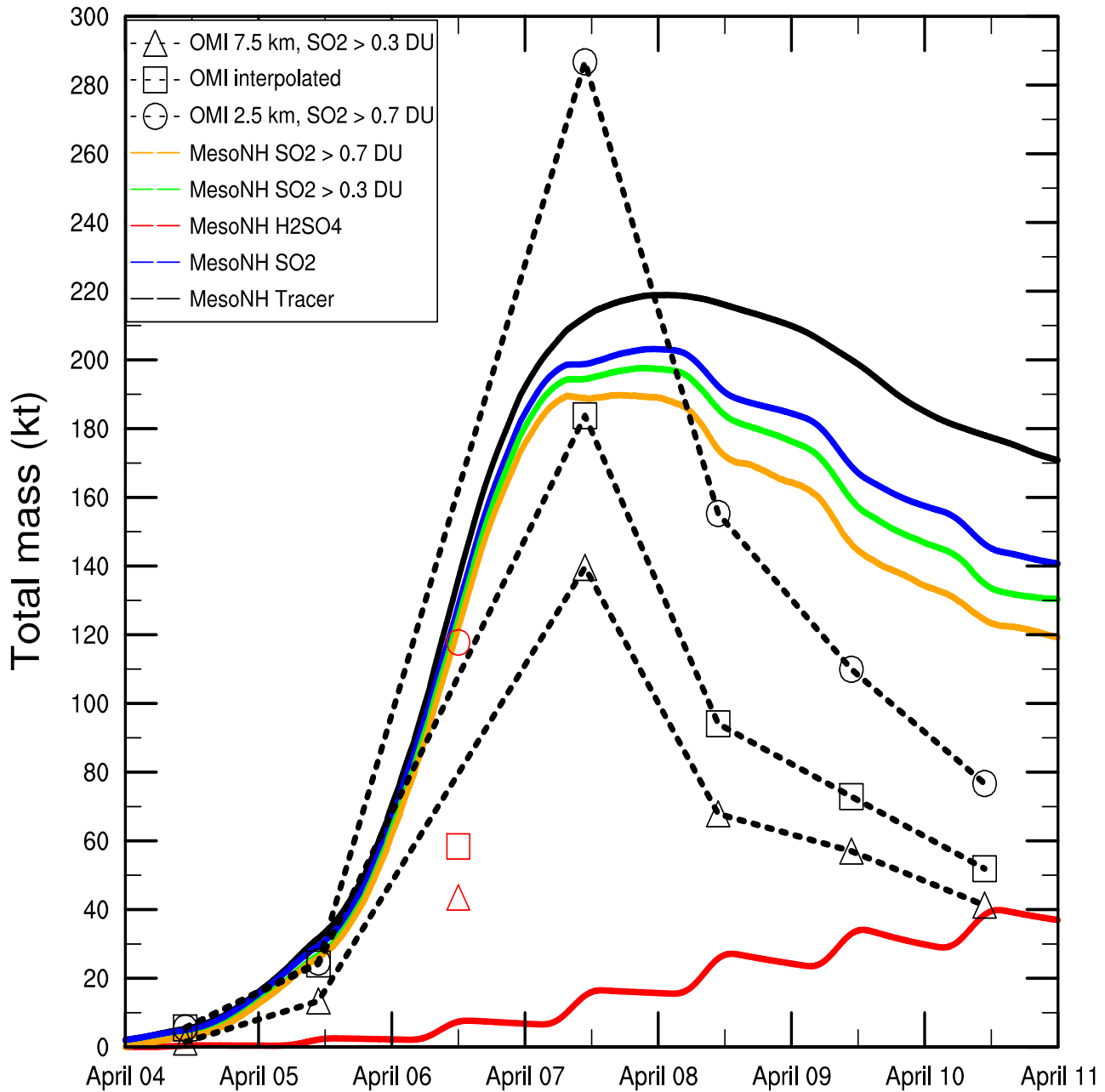


**Fig. 8.** Sum of the mass (kt) simulated by MesoNH on the whole domain (solid lines) and observed by OMI (dashed lines with triangles, squares and circles) between April 4 and April 11, 2007. Black, blue, green, yellow and red solid lines correspond to the passive tracer, the  $\text{SO}_2$ , the  $\text{SO}_2$  where the mass burden is higher than 0.3 DU, the  $\text{SO}_2$  where the mass burden mass is higher than 0.7 DU, and the  $\text{H}_2\text{SO}_4$ , respectively. Black triangles, circles and squares correspond to the OMI total mass given by TRM, TRL and weighted between TRL and TRM, respectively. Red triangles, circles and squares represent underestimated OMI values.

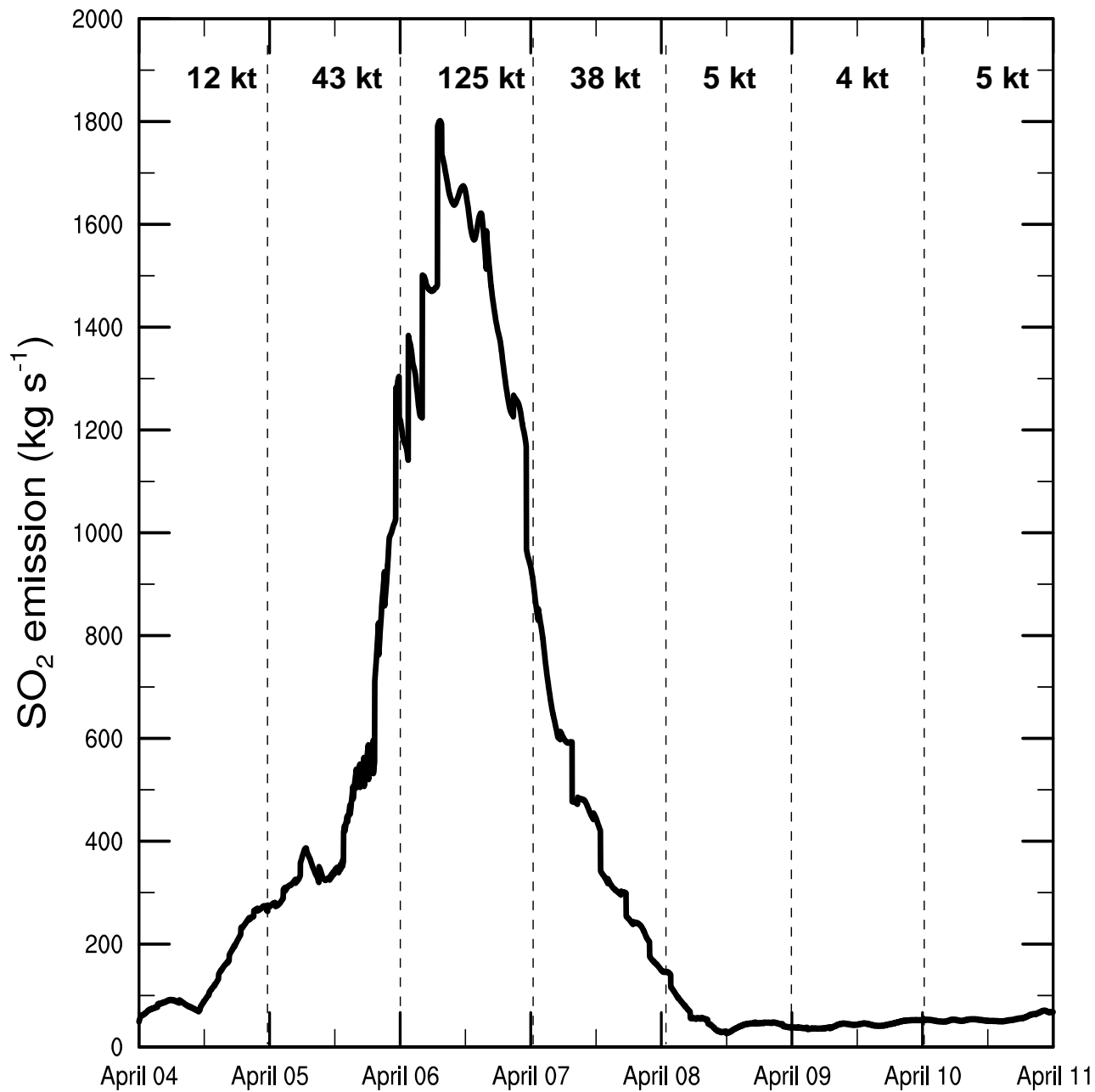


**Fig. 9.** Evolution of the SO<sub>2</sub> emission ( $kg.s^{-1}$ ) estimated by MesoNH between April 4 and April 11, 2007. Values along the top correspond to daily mass of SO<sub>2</sub> (kt) emitted during the period.